SUMMARY OF CALCULATIONS FOR THE INTERMEDIATE-SPECTRUM CELLS OF ZEBRA 8 USING THE ECCO CODE

D Hanlon
N T Gulliford

Experimental Reactor Physics Department
Safety And Performance Division
Winfrith Technology Centre

June 1993

1 Introduction

ZEBRA is a versatile zero-power fast reactor located at Winfrith Technology Centre. It is used predominantly to validate the calculational methods and cross-section data used for predictions for fast power reactors.

ZEBRA 8 included a series of seven test zones of plate cells with k-infinity values close to unity and fast/intermediate neutron spectra.

The experimental data obtained were originally used with the MURAL collision probability code[1] to derive the adjusted FGL5 data set for fast reactor calculations[2,3]. The all-uranium test region, ZEBRA 8H[4], was also studied in French and West German reactors and led to an international standard for data tests[5]. The experiments have also been used for the validation and testing of the MONK Monte-Carlo Code[6,7].

Recently the Core 8 data has been placed into SNEDAX, the European Fast Reactor Database, and calculations have been carried out using the European Cell Code (ECCO)[8] using the JEF2.2 Nuclear Data Library[9]. This note describes the calculational results and makes comparisons with the experimental results and the earlier MURAL/FGL5 study.

2 Assembly Design

Each version of ZEBRA 8 comprised a test region about 600mm in diameter and 600mm high, enclosed axially and radially in a ^{235}U-fuelled driver 80mm thick which, in turn, was surrounded by a natural uranium reflector about 300mm thick. Each region consisted of plates 51mm square, ranging in thickness from 1.6mm to 76mm, (the thicker plates being confined to the reflector). The plates were stacked horizontally in close fitting stainless-steel square-sectioned sheaths about 3m long and with a 0.76mm wall thickness.

There were 9 control rods in the driver region. The lower portions of the rods contained cells similar to those in the driver, so that when raised, they were effectively indistinguishable from normal driver elements. When lowered 8 of these rods introduced boron into the driver. The ninth, in which aluminium replaced the boron, was used for fine control.

The test region cells, which were repeated axially, are shown in Reference 10. The 37% enriched uranium metal, natural uranium metal, graphite and stainless steel plates were all nominally 3.175mm thick. The plutonium metal plates were also 3.175mm thick and had an inner copper can and an outer steel can. The mixed-oxide, natural-uranium oxide and sodium plates were all nominally 6.35mm thick and had stainless steel cans.

Descriptions of all the plates in the cells and the fuel element sheath are given in Refernce 10, in sufficient detail to allow the cells to be modelled in other codes if required. A more detailed layout of one of the cells showing the cans of the plates and the sheath is seen in Figure 1. For each test cell the constituents were adjusted to give a k-infinity close to unity.

Figure 2 shows the assembly layout for the first test region cell. The number of driver elements varied for each test region, so that with all the control rods fully raised, the

assembly was just super-critical. Particular care was taken in the design of the assemblies to minimise any tilts in flux distribution across the test regions.

3 Measurement of k-infinity.

The null reactivity technique to establish when k-infinity of a test region is unity was developed at Hanford for thermal lattices[11]. It was subsequently used for intermediate spectra in the HECTOR reactor at Winfrith[12] and the first measurements in a fast spectrum were made in the DIMPLE reactor, also at Winfrith[13].

The method as applied at ZEBRA consisted of measuring the reactivity controlled by a cell, including the corresponding length of fuel sheath, relative to void at the centre of the test region. A similar measurement was made of the reactivity controlled by the plutonium or, in the case of 8H, the ^{235}Uin the cell. The two reactivities were then expressed as a ratio to avoid introducing the uncertainties associated with absolute reactivity calibrations into derivation of k-infinity. The reactivities were determined by compensating the movement of the calibrated fine control rod, the other eight control rods being fully raised.

Because the removal of a cell exposed the edges of plates in adjacent elements and the surfaces of the plates above and below the void, it was necessary to make measurements with different numbers of cells and with different axial boundaries. This enabled extrapolations to be made to the reactivity contributions from the changes in exposed areas of materials with strongly-resonant cross-sections were negligibly small.

In a finite-sized test zone, k-infinity for the test zone can be expressed as follows:-

$$\frac{(k_\infty)\ testzone}{(k_{eff})\ reactor} = 1 + Rm + \epsilon$$

R is the ratio of the worth of unit volume of the cell plus sheath relative to that of the fuel in the cell and m and ε are calculated factors, m relating to k∞ and ε allowing for the finite size of the test zone.

The method of extrapolation of the reactivity and the conversion of the extrapolated reactivity to k∞ using measured plutonium worths and calculated values of m and ε are described in detail in Reference 14.

The resulting k-infinity values varied between 0.971 and 1.030 with uncertainties of 0.003 to 0.007, (1 standard deviation). In most cases the contributions to these uncertainties from the reactivity measurements, the cell compositions and variations in the moisture content of graphite plates are small. The largest contributions were from the extrapolations and the calculations of m and E, although in some test regions there was also a significant contribution from flux asymmetries. The experimental results which appear in Table 2 are taken from References 4 and 15. In assessing the errors, a larger uncertainty in cell composition has been used than in Reference 15. This is in line with the later assessment in Reference 4. Details of the errors are given in Reference 16.

4 Measurement of Reaction-Rate Ratios.

Reaction-rate ratios were measured in the cells at the centre of the test region using foils. the methods used are described in Reference 16 and were in principle based on those used in thermal reactor spectra, where recent measurements are described in detail in Reference 17. Thus fission ratios were measured by comparing fission-product γ-activities above a threshold of 1.28 MeV and expressing those in terms of fission ratios from the different isotopes by comparison with calibrated fission chambers. The capture rate in ^{238}U (C8) relative to fission in ^{239}Pu (F9) or ^{235}U (F5) was measured by comparing foil activities with those irradiated in the NESTOR thermal column. In this case the fission measurements were are described above, while C8 was measured by comparison of γ-X ray coincidences from ^{239}Np decay at about 105 KeV. Plutonium, mixed-oxide, UO_2 and uranium metal plates were modified to allow the insertion of vertical foils which sampled the reaction rates through the thickness of plutonium or uranium region, at the plate centres. Reaction-rates were only determined where the isotope was present. Thus F9 was measured in the plutonium and mixed-oxide plates, F8 and C8 in the mixed-oxide, UO2 and uranium plates, and F5 in the uranium plates in 8H.

Supporting measurements of F8/F5 fission rates were made using solid-state track recorders. Checks of capture-to-fission ratios were also carried out in which absolute ^{238}U capture rate obtained via an $^{241}Am/^{239}Np$ source was related to an absolute fission rate via a calibrated fission chamber. These supplementary measurements and the good agreements found are described in Reference 16.

Small corrections for the radial variations of reaction-rates through the plates were obtained from measurements. Calculated corrections derived in a similar way to those for k-infinity were applied to the reaction-rate ratios to allow for the finite size of the test zones - see Reference 14.

The standard deviations in the measured reaction-rate ratios are about 2% [16]. For the fission ratios, these arise mainly from the uncertainties in the fission chamber deposit masses and bias corrections, although there are also significant contributions from radial reaction-rate variations in the plates, foil mass calibration and counting statistics. For the capture-to-fission ratio, the contributions are from the foil masses, the measured fission ratio between the test zone and the thermal column, resonance shielding of foils, radial variations in the reaction rates in the plate, with the main contribution coming from the ratio of capture and fission cross-sections in the thermal column.

The values for the fission-ratios and the associated uncertainties quoted here are from References 4 and 15. For the capture-to-fission ratio the thermal comparison results are from References 4 and 15 and the absolute method results are from Reference 16. Where the results from both methods are available (all except 8A and 8B) the mean of the two is quoted here. No attempt has been made to bring reaction-rate results in line with current nuclear data recommendations, eg half-lives and thermal cross-section ratios. The changes would be small and well within the experimental errors.

5 The ECCO Models

Each of the Core 8 cells were exported from SNEDAX using the standard EXECCO export module to produce a 3D ECCO slab model. The model used for these experiments is a stack of square slabs which may have different thicknesses but identical lateral dimensions. Each slab is split into an inner and outer region by a square boundary, coaxial with the outer boundary. The inner square can be of a different size in each slab. The export module exports the slab dimensions and the region definitions. Each different region has its own composition data. The outer region of each slab is set to the dimensions of the average pitch in ZEBRA, namely 5.42544cm. The material compositions in this region are smears containing air-gaps, sheath and any clad material. In the same way as in the MURAL 3D models. The 3D model for the 8F/2 cell is shown in Figure 3.

Due to the large size of the code and nuclear data it was necessary to reduce the number of regions in each cell. This was achieved by combining like regions, eg the graphite plates in A/2, the natural uranium plates in B, C/2, D, E and H, and the sodium cans in D and E. In addition the two types of steel in C/2 were averaged and included as one region. To further reduce the cell models they were converted to half-plan wherever possible. Due to the space limitations, for cell 8E it was necessary to leave out the isotopes of Phosphorus and Sulphur. These elements occur in very small quantities as impurities in the cladding.

Each of the cases used the following ECCO reference route:

i) Homogeneous cell
172 groups
All elements

ii) Heterogeneous cell
172 groups
All elements

iii) Heterogeneous cell
Fine groups
Selected Elements

iv) Homogeneous cell
33 groups

v) Homogeneous cell
1 group

The calculational inputs are provided in Reference 10.

6 Results

All the k-values from ECCO using JEF2.2 data are shown in Table 1. The Table also gives the experimental k-values and those obtained from the MURAL collision-probability code calculations with FGL5 data, which are taken from References 18 and 19.

Table 2 shows the percentage differences between the experimental and calculated k_∞-values. The ECCO results show differences at or above two standard deviations in cells A/2, C/2, E and H. These values may be significant but are not entirely surprising since JEF2.2 is unadjusted data.

Table 3 summarises the microscopic C8/F9 (or C8/F5 for cell 8H) ratios from ECCO, MURAL and measurement. The differences are noted in Table 4. The ECCO calculations show that all cases are within two standard deviations, except cell 8F/2 which is closer to three standard deviations. In all cases the value of C8/F9 is over-predicted.

Table 5 similarly compares the calculated and measured fission ratios F8/F9 (or F8/F5 for 8H). The differences between calculation and experiment are summarised in Table 6. The ECCO calculations show that all cases are within two standard deviations. In all cases the value of C8/F9 is over-predicted, except in cell 8F/2 which is under-predicted.

For the MURAL calculations the k_∞-values show good agreement with experiment, only in 8F/2 is the difference between calculation and experiment greater than two standard deviations. The C8/F9 ratios from the MURAL models agree with experiment within the experimental errors, with the exception of 8F/2 where the difference is two standard deviations. The F8/F9 ratios from MURAL are also in agreement with measurement within the experimental uncertainties, except 8H where the difference is just greater than two standard deviations.

When comparing the root mean square deviations in both ECCO and MURAL calculations the only significant difference to note is in the k_∞-values. ECCO gives a root mean square deviation of 1%, MURAL gives 0.52% compared to the experimental RMS uncertainty of 0.46% for the seven experiments.

7 CONCLUSIONS

Calculations for the cells from the ZEBRA 8 Assembly with k-infinities close to unity have been run using ECCO and its associated JEF2.2 Nuclear Data. The models have been produced by exporting information stored in the European Fast Reactor Database SNEDAX.

The agreement between the results for k-infinity from ECCO/JEF2.2 and measurement are reasonably good, differences varying between -0.016 and +0.008. Although the MURAL/FGL5 results are significantly better, this is perhaps expected since the FGL5 Nuclear Data was adjusted to a data set which included these measurements.

REFERENCES

1 J D McDougall. The use of the 2000 Energy Group Reactor Physics Code MURAL in the Investigation of Special Effects in Fast Reactors. International Symposium on Physics of Fast Reactors. Tokyo October 1973. Paper A32.

2 J L Rowlands et al. The production and Performance of the Adjusted Cross-section Set FGL5. Ibid. Paper A30.

3 M J Grimstone, J L Rowlands. Collision Probabilities for Plate Geometry Cells with an Approximate Treatment of Plate Edge Regions. AEEW - R 1923.

4 B L H Burbidge et al. ZEBRA 8H, A U235/U238 Fast Reactor Benchmark. AEEW - R 888.

5 M Darrouzet et al. Studies of Unit k∞ Lattices in Metallic Uranium Assemblies ZEBRA 8H, SNEAK8, ERMINE and HARMONIE UK. International Symposium on Physics of Fast Reactors, Tokyo, October 1973. Paper A28.

6 MONK 6 Supporting Documentation. AEEW - R 2248

7 D Hanlon et al. Calculations for the Intermediate-Spectrum Cells of ZEBRA 8 Using the MONK Monte-Carlo Code. AEEW -R 2245

8 J D Tullett, M J Grimstone. ECCO - The European Cell Code (Version 4) User Manual. CFSM/P(90)97. April 1990.

9 F Helm, A Schröder. SNEDAX: A Databank for Fast Critical Experiments. ANS Conference Paper. 1992

10 D Hanlon, N T Gulliford. Calculations For The Intermediate-Spectrum Cells of ZEBRA 8 Using The ECCO Code. AEA-RS-1239. April 1993.

11 D J Donahue et al. Determination of k-infinity from Critical Experiments with the PCTR. Nucl Sc Eng 4, 297, (1958).

12 W N Fox et al. An Experimental Study of the Integral Properties of U235 and Pu239 in an Intermediate Energy Spectrum and Comparison with Theoretical Prediction. AEEW - R 586.

13 M J Arnold et al. Experimental Physics Studies of Steam-Cooled Fast Reactor Lattices. AEEW - R 560.

14 D Wardleworth. The Interpretation of Measurements in ZEBRA Core 8. AEEW - R 893.

15 G Ingram. Classified Winfrith Report.

16 J E Sanders et al. A Review of ZEBRA Techniques for the Measurement of Reactivity Parameters, Reaction Rate Ratios and Spectra, International Symposium on Physics of Fast Reactors. Tokyo, October 1973. Paper B18.

17 M F Murphy. Fast Fission Ratio and Relative Conversion Ratio Measurements in Gadolinium Poisoned Water Moderated UO_2 Lattices. AEEW - R 1714.

18 Miss P A Smart, G Ingram. ZEBRA Core 8 FGL5 Calculations. Private Communication.

19 M J Grimstone, J L Rowlands. Collision Probabilities for Plate Geometry Cells with an Approximate Treatment of Plate Edge Regions. AEEW - R 1923.

Table 1

Comparison of k∞ from ECCO, MURAL and Experiment

	k∞		
ZEBRA 8 Cell	ECCO/JEF2.2	MURAL 3D	Experiment
A/2	0.979	0.9924	0.992±0.006
B	1.001	1.0047	1.001±0.003
C/2	0.972	0.9813	0.986±0.004
D	0.970	0.9763	0.973±0.004
E	0.990	1.0016	1.006±0.007
F/2	0.968	0.9804	0.971±0.004
H	1.039	1.0250	1.030±0.003

Table 2

Comparisons of $(\frac{C-E}{E})\%$ for k∞

Cell	ECCO 3D	MURAL 3D
A/2	-1.3±0.6	0.0±0.6
B	0.0±0.3	0.4±0.2
C/2	-1.4±0.4	-0.5±0.4
D	-0.3±0.4	0.3±0.4
E	-1.6±0.7	-0.4±0.7
F/2	-0.3±0.4	1.0±0.4
H	0.8±0.3	-0.5±0.3
RMS Value	1.0%±0.46%	0.52%±0.46%

Table 3

Comparison of C8/F9 Microscopic Reaction-Rate Ratios from ECCO, MURAL and Experiment

Cell	ECCO 3D	MURAL 3D	Experiment
8A/2	0.1279	0.1240	0.1241±0.0028
8B	0.1262	0.1251	0.1257±0.0026
8C/2	0.1306	0.1285	0.1296±0.0016
8D	0.1289	0.1288	0.1275±0.0023
8E	0.1253	0.1237	0.1239±0.0020
8F/2	0.1553	0.1516	0.1504±0.0020
8H*	0.1153	0.1178	0.1136±0.0017

* For 8H, the ratios are C8/F5.

Table 4

Comparisons of $(\frac{C-E}{E})\%$ for $\frac{C8}{F9}$ Reaction-Rate Ratios

Cell	ECCO 3D	MURAL 3D
8A/2	3.1±2.3	-0.1±2.3
8B	0.4±2.1	-0.5±2.1
8C/2	0.8±1.2	-0.8±1.2
8D	1.8±1.8	1.0±1.8
8E	1.2±1.6	-0.2±1.6
8F/2	3.3±1.3	0.8±1.3
8H*	1.5±1.5	3.7±1.5
RMS Value	2.0%±1.73%	1.5%±1.73%

* For 8H, the ratios are C8/F5.

Table 5

Comparison of F8/F9 Microscopic Reaction-Rate Ratios from ECCO, MURAL and Experiment

Cell	ECCO 3D	MURAL 3D	Experiment
8A/2	0.01662	0.01626	0.01632±0.0051
8B	0.02124	0.02087	0.02124±0.0059
8C/2	0.01137	0.01137	0.01137±0.0036
8D	0.01788	0.01851	0.01788±0.0063
8E	0.01719	0.01769	0.01719±0.0074
8F/2	0.01983	0.01852	0.01983±0.0065
8H[(1)]	0.02278	0.02329	0.02278±0.0045

* For 8H, the ratios are F8/F5.

Table 6

Comparisons of $(\frac{C-E}{E})\%$ for $\frac{F8}{F9}$ Reaction-Rate Ratios

Cell	ECCO 3D	MURAL 3D
8A/2	1.8±3.1	-0.4±3.1
8B	1.7±2.8	-1.7±2.8
8C/2	3.0±3.2	0.0±3.2
8D	4.5±3.5	3.5±3.5
8E	3.5±4.3	2.9±4.3
8F/2	-5.9±3.3	-6.6±3.3
8H*	2.9±2.0	2.2±2.0
RMS Value	3.6%±3.2%	3.2%±3.2%

* For 8H, the ratios are F8/F5.

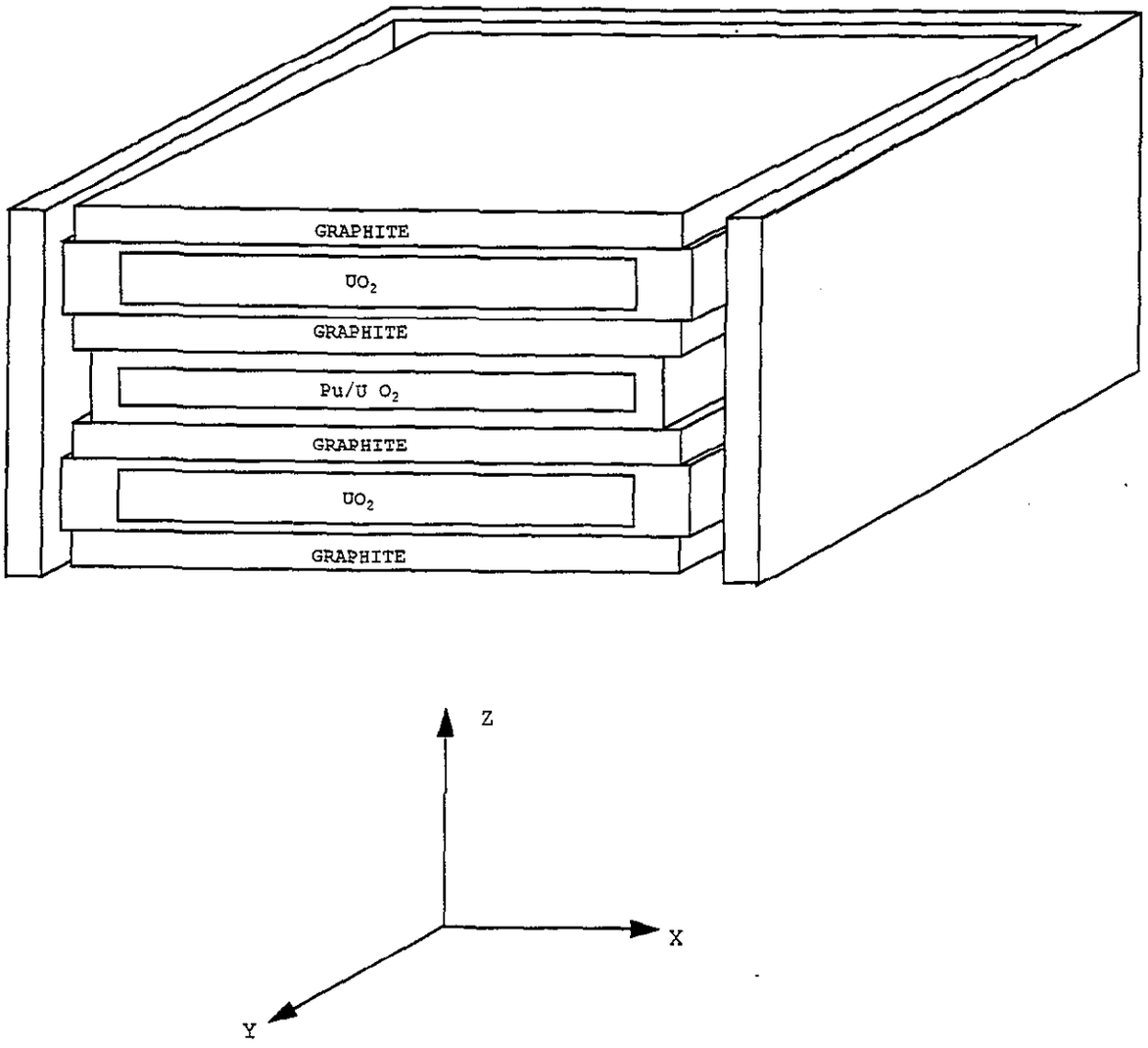

FIGURE 1. CUT-AWAY DIAGRAM OF CELL 8F/2

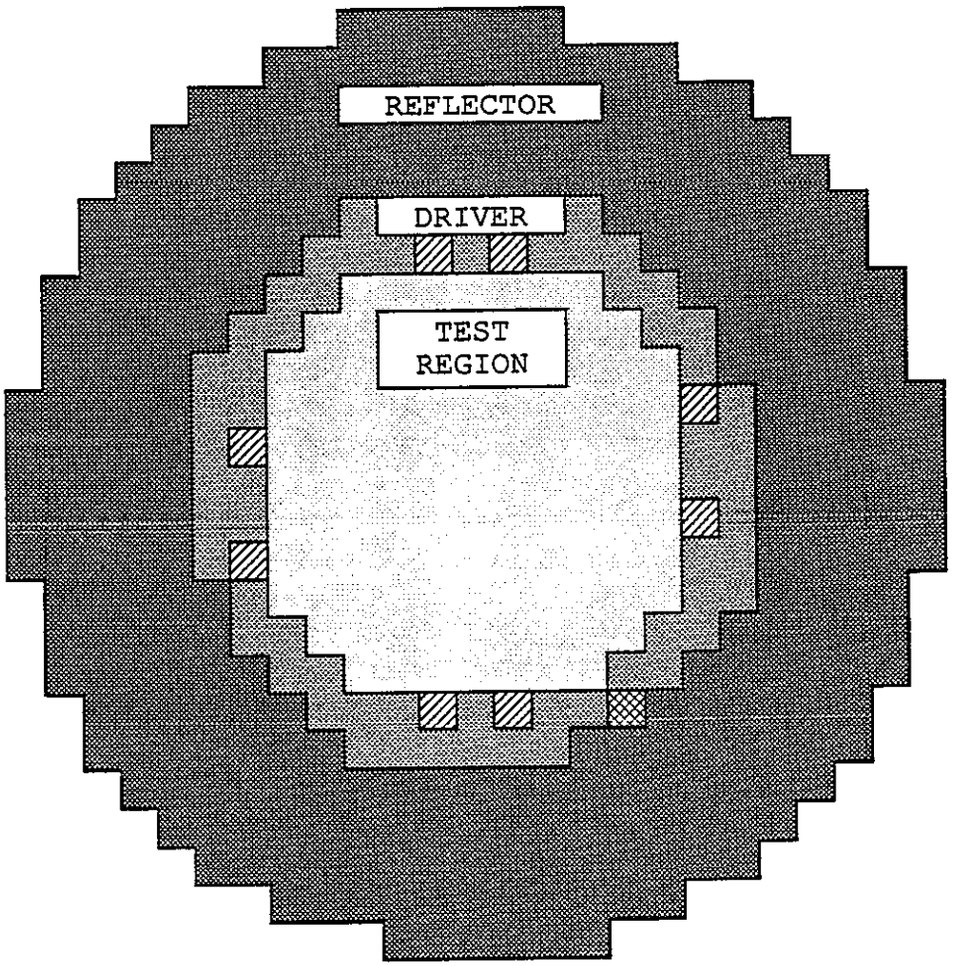

FINE CONTROL ROD

FIGURE 2. CORE 8A/2

Graphite

Natural UO_2

Natural UO_2 Can and Sheath

Natural UO_2 Core

Pu/U O_2 Can

Pu/U O_2 Can and Sheath

Pu/U O_2 Core

Sheath

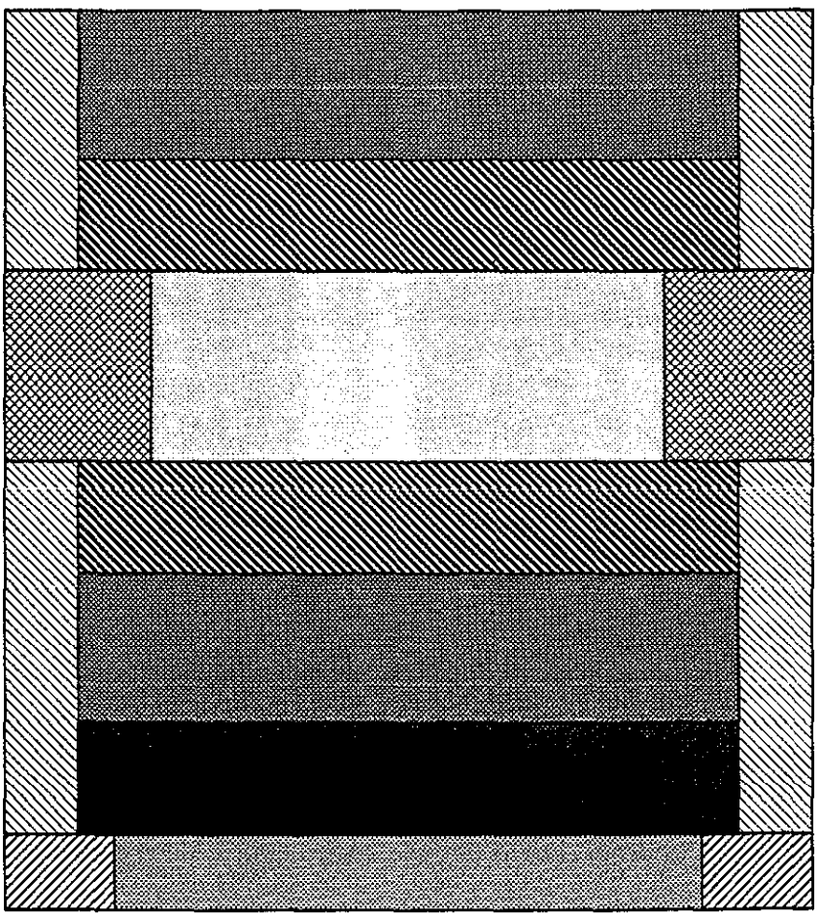

Notes:

1) The model is split into 2 radial regions.

2) The air gaps are smeared into the Sheath/Sheath and Can compositions

FIGURE 3. 3-D MURAL MODEL OF HALF CELL 8F/2